DUAL LAYER SLOT COATING

Oldrich Joel Romero
Department of Mechanical Engineering / Pontificia Universidade Catolica do Rio de Janeiro / Rio de Janeiro, RJ, 22453-900, Brazil.
oldrich@mec.puc-rio.br

Márcio da Silveira Carvalho
Department of Mechanical Engineering / Pontificia Universidade Catolica do Rio de Janeiro / Rio de Janeiro, RJ, 22453-900, Brazil.
msc@mec.puc-rio.br

Abstract. *The mathematical modeling of free surface flows requires solving free boundary problems. Specifically in a two-layer slot coating process, where two liquids are deposited in a continuous substrate, two liquid-air interfaces exist upstream and downstream of the feed slots and one liquid-liquid interface between the two miscible coating liquids. The topology of these evolving interfaces changes during the course of events, are unknown a priori and depends on the process operating conditions. Elliptic mesh generation technique (de Santos, 1991), is used to compute the upstream and downstream free surfaces. The interlayer position is obtained solving a purely convective equation in the full domain for a scalar field. This new unknown allows us to use different properties (density or viscosity) for each liquid. This formulation is similar to the level set method of Osher and Sethian (1988). The unknown flow domain (physical) is mapped into a fixed domain (computational). The system of equations, with appropriate boundary conditions, for a two-dimensional viscous liquid flow is solved in coupled form by the Galerkin and Petrov Galerkin / Finite Element Methods. The set of non-linear algebraic equations for the finite element basis functions is solved by Newtont's method. Different viscosity ratio (viscosity upper layer liquid / viscosity lower layer liquid), vacuum pressure and flow rates (or coating thickness) were used in order to investigate the downstream static contact angle, dynamic contact line and the flow field behaviors.*

Keywords: *two-layer slot coating, free surfaces, level set method, elliptic mesh generation, finite element method.*

1. Introduction

An enormous range of manufactured products involves layers deposited as a liquid and then solidified on a solid surface. Frequently, the coating stage of a manufacturing process is significant in cost, time involved and the level of technology required for the production. To be competitive in the marketplace, all aspect of the manufacturing must be efficient and maintain an acceptable level of quality control.

Many products require two or more superposed layers. Multiple layers can be coated in two ways: (i) in tandem, the bottom layer is coated first and dried, then the next layer is applied; or (ii) simultaneously, where the liquids are deposited at the same time. Two liquid layers can be coated simultaneously by employing an applicator die which has two feed slots each delivering the liquid of a separate layer. The liquids are keep apart until just before application onto the substrate. The reason for that is to avoid inter-diffusion or chemical reaction. Coating multiple layers simultaneously is generally more difficult and less well understood than coating single layers.

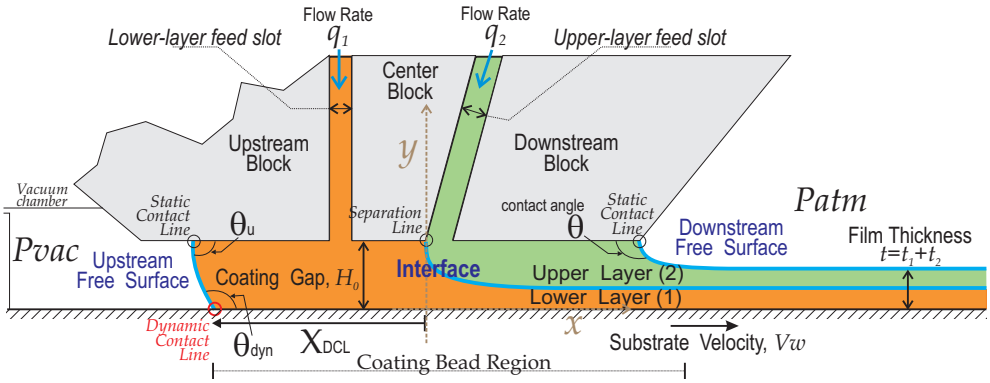

Figure 1. Side profile with features of the two-layer slot coating.

Figure 1 shows a typical configuration of a two-layer applicator die and substrate. A meniscus is formed at the upstream end by the lower-layer liquid and air. Usually a reduced pressure or "vacuum" is used to sustain the coating bead at high substrate speeds. A meniscus is also formed at the downstream end between the upper-layer liquid and the ambient air. In between, the bulk of the upper-layer and lower-layer liquids are separated by a slim interdiffusion zone of each liquid called interlayer or interface. The liquid in the gap, bounded by the meniscus forms the coating bead region.

2. Mathematical Formulation

The important variables in a two-layer slot coating includes surface and interfacial tension, viscosity, flow rate, density, gravity, vacuum level, and geometrical parameters (as coating gap, die shape, corners, etc.). In this study, the effect of the surface tension, viscosity and flow rate of each liquid, and vacuum level on the flow are analyzed.

The flow in the two-layer slot coating, considered two-dimensional, inertialess, isothermal, steady-state, with no-phase-change, was described by mass and momentum conservation equations for each layer. The Newtonian liquids are miscible, *i.e.*, there are no interfacial tension in the inter-layer.

The Navier-Stokes equations for each liquid are:

$$\nabla \cdot [-p + \mu_1(\nabla \mathbf{v}_1 + \nabla \mathbf{v}_1^T)] = 0, \qquad \nabla \cdot \mathbf{v}_1 = 0, \tag{1}$$

$$\nabla \cdot [-p + \mu_2(\nabla \mathbf{v}_2 + \nabla \mathbf{v}_2^T)] = 0, \qquad \nabla \cdot \mathbf{v}_2 = 0, \tag{2}$$

where p is the pressure, $\mathbf{v}$ the velocity, μ is the viscosity, sub-indices "1" and "2" identify the liquid 1 and liquid 2, or lower and upper layer, respectively.

Appropriate boundary conditions are necessary to solve the system of equations Eqs. (1) and (2).

2.1 *Boundary Conditions*

The boundaries of the flow domain are identified in Fig. 2, and are the following:

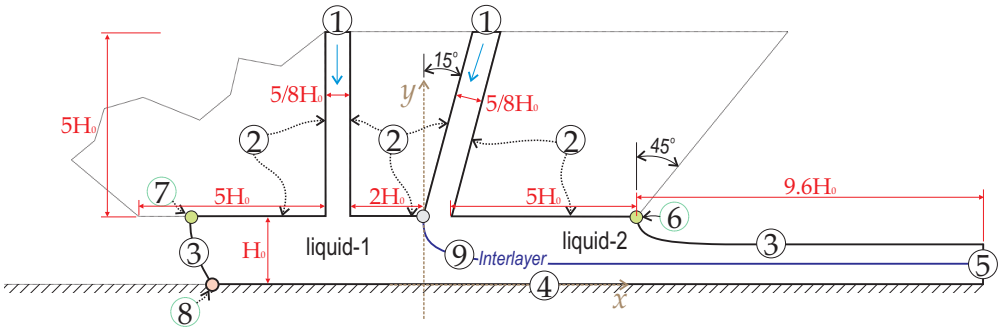

Figure 2. Labels for the boundary conditions in two-layer slot coating and domain dimensions in units of slot gap $H_0 = 100\mu m$, similar to used by Musson (2001). The location of the 2D cartesian coordinates is also shown.

1. At the two inflow planes, that is, at the die feeding slot, the flow is assumed to be fully developed parallel rectilinear flow, where a Couette-Poiseuille velocity profile is prescribed.

$$u = -\frac{6q}{H_0}\left[\left(\frac{x}{H_0}\right) - \left(\frac{x}{H_0}\right)^2\right], \quad v = 0, \tag{3}$$

where q is the flow rate feed to the coating die. It defines the thickness of the liquid layer deposited onto the substrate: $t_{1,2} = q_{1,2}/V_w$, ("1" is for sub layer and "2" for upper layer liquid); H_0 is the gap between the die and the substrate.

2. The no-slip and no-penetration conditions applies at the die walls.

$$\mathbf{v} = \mathbf{0}. \tag{4}$$

3. At the free surfaces, the traction in the liquid balances the capillary pressure and there is no mass flow rate across the gas-liquid interface. This is the force balance and kinematic condition.

$$\mathbf{n}_{fs} \cdot \mathbf{T} = \frac{1}{Ca}\frac{d\mathbf{t}_{fs}}{ds} - \mathbf{n}_{fs}p_{air}, \tag{5}$$

$$\mathbf{n}_{fs} \cdot \mathbf{v} = 0, \tag{6}$$

where $\mathbf{T} = -p\mathbf{I} + \mu_{1,2}(\nabla \mathbf{v} + \nabla \mathbf{v}^T)$ is the stress tensor in the Newtonian liquid; $Ca \equiv \mu_{1,2}V_w/\sigma$ is the capillary number; $d\mathbf{t}_{fs}/ds$ represents the curvature of the meniscus; $\mathbf{t}_{fs}$ and $\mathbf{n}_{fs}$ here are the local unit tangent and unit

normal to the free surface and p_{air} is the pressure of the air. At the downstream free surface, the air pressure is usually atmospheric, that is $p_{air} = P_{atm}$. At the upstream liquid gas-liquid interface, vacuum is usually applied in order to stabilize the coating bead, that is $p_{air} = P_{vac}$.

4. In the moving substrate, the no-slip and no-penetration conditions are applied.

$$u = V_w, \quad v = 0, \tag{7}$$

V_w is the substrate velocity.

5. At the outflow fully developed flow is applied.

$$\mathbf{n} \cdot \nabla \mathbf{v} = 0, \tag{8}$$

$\mathbf{n} \cdot \nabla$ is here the directional derivative parallel to the substrate.

6. The downstream static contact line is pinned to the sharp edge of the die. That is, the position (x_d, y_d) of the downstream static contact line is fixed.

$$(x_d, y_d) = (X_{corner}, Y_{corner}). \tag{9}$$

7. The upstream static contact line is free to slide along the die face. This is, the vertical coordinate, y_u, of the upstream static contact line is fixed and the upstream static contact angle, θ_u, of the free surface with the die face has to be specified. In this work the angle was set in $\theta_u = 100^o$.

$$y_u = H_0, \qquad \mathbf{n}_w \cdot \mathbf{n}_{fs} = cos(\theta_u), \tag{10}$$

$\mathbf{n}_w$ is the unit vector normal to the wall.

8. At the web surface the liquid translates with the web except near the locations where the liquid first appears to contact the web. This sub-microscopic region is called the dynamic contact line, where evidences points a very thin film of air being entrained when the coating speed is high and to that air film breaking down and dissolving within around $100\mu m$ of the dynamic contact line. In this short region the Navier slip condition was used instead of the no-slip condition and a dynamic contact angle $\theta_{dyn} = 110^o$ was specified.

$$\frac{1}{\beta}\mathbf{t}_w \cdot (\mathbf{v} - V_w\mathbf{i}) = \mathbf{t}_w \cdot (\mathbf{n}_w \cdot \mathbf{T}), \qquad \mathbf{n}_w \cdot \mathbf{n}_{fs} = cos(\theta_{dyn}), \tag{11}$$

where β is the slip coefficient, $\mathbf{t}_w$ is the unit vector tangent to the wall. Without the slip condition there is a non-integrable singularity in shear stress. For a better description of the flow in this region, a contact angle as a function of a capillary number would be more appropriate.

9. All along the interface, the forces exerted by pressure and viscous traction must balance. Capillary pressure is not acting because the liquids -considered miscible- have no interfacial tension. The liquids in contact have a thin layer of interdiffusing components of liquids 1 and 2. The interlayer condition is

$$\mathbf{n}_{if} \cdot \mathbf{T}_1 = \mathbf{n}_{if} \cdot \mathbf{T}_2, \tag{12}$$

where $\mathbf{n}_{if}$ is the unit vector normal to the interlayer. This normal stress balance can be resolved as $(p_1 - p_2)\mathbf{n}_{if} = (\mu_1 - \mu_2)(\partial v_n/\partial s_n)\mathbf{n}_{if}$, where s_n arclength along a coordinate normal to the interface. When the normal viscous stresses at the interface are appreciable, the pressure is discontinuous across the interface unless the liquids on either side have identical viscosities.

2.2 *Dimensionless Parameters*

The dimensionless parameters that governs the problem are: *(i)* Capillary number $Ca \equiv \mu_2 V_w/\sigma$, which measures the ratio of viscous to capillary forces at the downstream meniscus, μ_2 is the viscosity of the upper layer liquid and was set constant to $\mu_2 = 20cP$, V_w is the substrate velocity, constant at $V_w = 3m/s$, and σ the liquid surface tension; *(ii)* Dimensionless vacuum pressure $Vac \equiv P_{vac}H_0/\sigma$; *(iii)* Gap-to-thickness ratio $h \equiv H_0/t$, H_0 is the separation of the die land from the moving substrate and is set to $H_0 = 100\mu m$; $t = t_1 + t_2$ is the total wet coating thickness deposited onto the substrate; *(iv)* Viscosity ratio $\mu_R \equiv \mu_2/\mu_1$, viscosity of the top layer over bottom layer; *(v)* Flow rate ratio $q_R \equiv q_2/q_1$, is a measure of the flow rate en each layer, and represents the wet film thickness ratio.

3. Solution Method

3.1 *Formulation of the Free Boundary Problem*

Because of the free surface, the flow domain at each set of parameter values is unknown *a priori*. To solve the free boundary problem by standard techniques for boundary value problems, the set of differential equations and boundary conditions posed in the unknown domain Ω (with boundaries Γ) has to be transformed to an equivalent set defined in a known reference domain $\overline{\Omega}$ (with boundaries $\overline{\Gamma}$). This can be done with a mapping $\mathbf{x} = \mathbf{x}(\boldsymbol{\xi})$ that connects the two domains, as is shown in Fig. 3. The unknown physical domain is parameterized by the position vector $\mathbf{x}$ and the reference domain, by $\boldsymbol{\xi}$, as described in detail by de Santos (1991), who showed that a functional of weighted smoothness can be used successfully to construct the sorts of maps involved here.

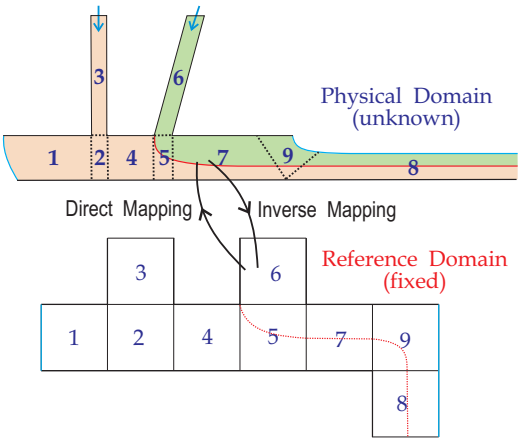

Figure 3. Mapping from physical to reference domain.

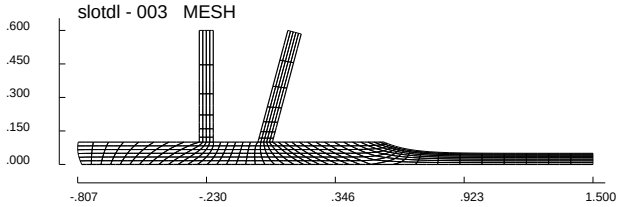

Figure 4. Representative mesh with 367 elements.

3.1.1 Elliptical Mesh Generation: Capturing the Gas-Liquid Interfaces

The inverse of the mapping that minimizes the functional is governed by a pair of elliptic differential equations identical to those encountered in diffusional transport with variable diffusion coefficients. The coordinates ξ and η of the reference domain satisfy:

$$\nabla \cdot (\mathbf{D} \cdot \nabla \boldsymbol{\xi}) = 0, \tag{13}$$

where $\nabla \equiv \partial/\partial \mathbf{x}$ denotes differentiation in physical space, and $\mathbf{D}$ is the diffusivity-like adjustable tensor that serves to control the gradients in coordinate potentials, and thereby the spacing between curves of constant ξ and of constant η. Selected subsets of these two sets of curves make up the sides of rectangular elements into which the reference domain is divided; their mapping back to the flow domain is a tessellation into quadrilateral elements (see Benjamin, 1994).

Boundary conditions are of course needed before the second-order partial differential equations, Eq. (13), can be solved. The solid walls and synthetic inlet and outlet boundary planes were specified as functions of the coordinates and along them stretching functions were used to distribute the terminii of the coordinate curves selected to serve as element sides. The free boundary – the gas-liquid interface or meniscus – is implicitly located by imposing the kinematic condition, Eq. (6). The discrete versions of the mapping equations are generally referred to as mesh generation equations.

3.1.2 The Two-Phase Flow: Tracking the Liquid-Liquid Interface

The liquid-liquid interface was determined solving a purely convective equation in all the domain for a new scalar field, "ϕ".

$$\mathbf{v} \cdot \nabla \phi = 0, \tag{14}$$

this equation, which is the steady version of the level set equation proposed by Osher and Sethian (1988), allows to know the concentration in each point of the domain.

Because it is a purely convective equation, boundary conditions are only necessary in the two inflow planes, label "1" in Fig. (2). For the liquid-1 (sub-layer) it was was set at $\phi = -1$, and for the liquid-2 (upper-layer) $\phi = +1$ was applied. The interlayer is where $\phi = 0$.

Viscosity is constant in each liquid and take on two different values, μ_1 or μ_2, depending of the sign of "ϕ" through the Heaviside function $H_\epsilon(\phi)$, hence we may write

$$\mu(\phi) = \mu_1[1 - H_\epsilon(\phi)] + \mu_2 H_\epsilon(\phi). \tag{15}$$

Sharp changes on pressure due to large viscosity ratios (or density ratios when considered) across the front can present numerical difficulties. To alleviate these problems the smoothed Heaviside function $H_\epsilon(\phi)$ is defined as:

$$H(c) = \begin{cases} 0 & \text{if } \phi < -\epsilon, \\ \frac{1}{2}[1 + \frac{\phi}{\epsilon} + \frac{1}{\pi} sin(\pi \frac{\phi}{\epsilon})] & \text{if } |\phi| \leq \epsilon, \\ 1 & \text{if } \phi > \epsilon, \end{cases} \tag{16}$$

here ϵ is the interface numerical thickness proportional to the finest spatial-mesh size Δx along the flow direction, a practical rule could be $\Delta x < \epsilon < 3\Delta x$. So, in this way the interface has a thickness of approximately $2\epsilon/|\nabla\phi|$.

Defining the velocity in analogous fashion, the system of equations given by Eqs. (1) and (2) can be combined into the following:

$$\nabla \cdot [-p + \mu(\phi)(\nabla \mathbf{v} + \nabla \mathbf{v}^T)] = 0, \qquad \nabla \cdot \mathbf{v}. \tag{17}$$

3.2 *Solution of the equation system by Galerkin and Petro-Galerkin / Finite Element Methods*

The weighted residual equations are obtained after multiplying each governing equation, Eqs. (17), (13) and (14) by weighting functions ψ^m, ψ^c, ψ^x and ψ^ϕ, integrating over the unknown flow domain Ω (bounded by Γ), applying the divergence theorem to the terms with divergences and mapping the integrals onto the known reference domain $\bar{\Omega}$ (bounded by $\bar{\Gamma}$):

$$R_i^{\mathbf{m}} \equiv \int_{\bar{\Omega}} [\nabla \psi_i^m \cdot \mathbf{T}] \; J \; d\bar{\Omega} - \int_{\bar{\Gamma}} \psi_i^m (\mathbf{n} \cdot \mathbf{T}) \left(\frac{d\Gamma}{d\bar{\Gamma}} \right) d\bar{\Gamma} = \mathbf{0}; \tag{18}$$

$$R_i^c \equiv \int_{\bar{\Omega}} (\nabla \cdot \mathbf{v}) \; \psi_i^c \; J d\bar{\Omega} = 0; \tag{19}$$

$$R_i^{\mathbf{x}} \equiv - \int_{\bar{\Omega}} \nabla \psi_i^x \cdot \mathbf{D} \cdot \nabla \boldsymbol{\xi} \; J \; d\bar{\Omega} + \int_{\bar{\Gamma}} \psi_i^x \mathbf{n} \cdot \mathbf{D} \cdot \nabla \boldsymbol{\xi} \left(\frac{d\Gamma}{d\bar{\Gamma}} \right) d\bar{\Gamma} = \mathbf{0}; \tag{20}$$

$$R_i^\phi \equiv \int_{\bar{\Omega}} (\mathbf{v} \cdot \nabla \phi) \; \psi_i^\phi \; J d\bar{\Omega} = 0; \tag{21}$$

$\mathbf{n}$ is the outward unit normal vector of the boundary Γ; $J = det\mathbf{J} = d\Omega/d\bar{\Omega}$ is the determinant of the mapping deformation gradient, and represents the ratio of magnitudes of infinitesimal elements of the physical to the reference domains. In eq. (18), $\mathbf{T} \equiv -p\mathbf{I} + \mu(\nabla \mathbf{v} + \nabla \mathbf{v}^{\mathbf{T}})$ is the stress tensor.

Each independent variable is approximated with a linear combination of a finite number of knows basis functions.

$$\mathbf{v} = \sum_j \widetilde{\mathbf{v}}_j \varphi_j^v, \quad \mathbf{x} = \sum_j \widetilde{\mathbf{x}}_j \varphi_j^x, \quad p = \sum_j \widetilde{p}_j \varphi_j^p, \quad \phi = \sum_j \widetilde{\phi}_j \varphi_j^\phi. \tag{22}$$

The basis functions used to expand the independent variables are: Lagrangian biquadratic polynomials for velocity φ^v, position φ^x and concentration φ^ϕ, and linear discontinuous for pressure φ^p. The Galerkin's method is applied to the equations of momentum, continuity and mesh generation, i.e. $\psi^m = \varphi^v$, $\psi^c = \varphi^p$ and $\psi^x = \varphi^x$. Streamline Petrov-Galerkin weighting functions are used in the level set equation, $\psi^\phi = \varphi^\phi + h_e \frac{\mathbf{v}}{||\mathbf{v}||} \cdot \nabla \varphi^\phi$, where h_e is the upwind parameter, taken as the characteristic size along the flow direction of the smallest element in the mesh.

3.3 *Solution of the non-linear system of algebraic equation by Newton's Method*

Once all the variables are represented in terms of the basis functions, the system of partial differential equations reduces to simultaneous algebraic non-linear equations for the coefficients of the basis functions of all the fields. The system of equations was solved by Newton's method with numerical evaluation of the Jacobian entries (central difference).

Because the finite element basis functions used are different from zero only over a very small portion of the domain, the Jacobian matrix is sparse and was stored in compressed sparse formats. In each iteration the linearized equation system was factorized into unit lower L and unit upper U triangular matrix by a frontal solver.

In order that the Newton process converged within 6 to 8 iterations at each successive new set of operating conditions, the initial estimates were generated by a pseudo-arc-length continuation method as described by Bolstad and Keller (1986). The tolerance on the L2-norm of the residual vector and on the last Newton update of each declared solution was set to 10^{-6}.

A mesh convergence analysis was done increasing the elements number until the solution changed by less that 1% between successive refinements. The domain was tessellated into 367 elements, as illustrated in Figure 4. This resulted in 9,116 simultaneous nonlinear equations.

4. Results

Solutions were computed at constant capillary number $Ca = 0.1$ and several viscosity ratio $\mu_R = \mu_2/\mu_1$ (top layer/bottom layer viscosity), flow rate ratio q_R, gap-to-thickness ratio H_0/t, and vacuum level Vac.

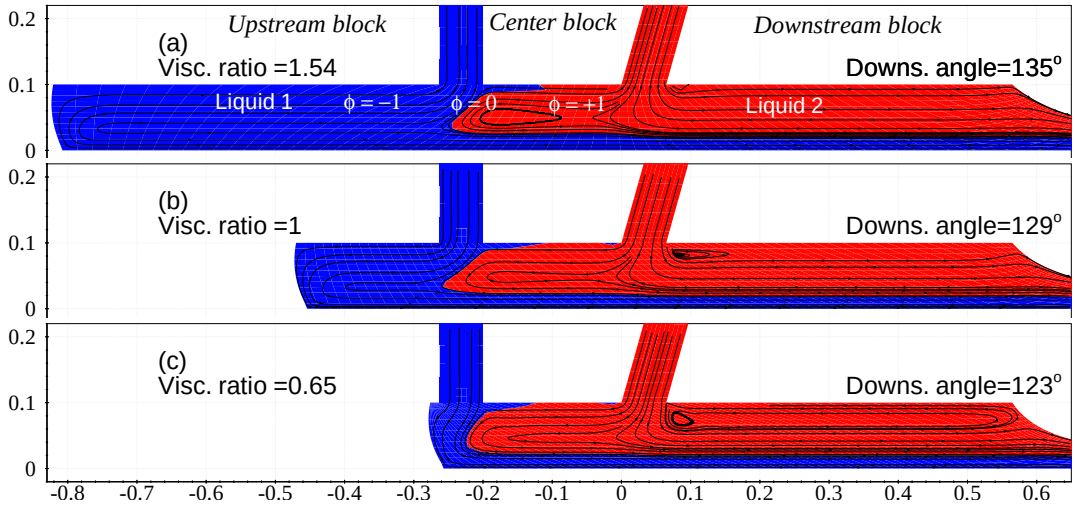

Figure 5. Flow field at different viscosity ratios ($\mu_R = \mu_2/\mu_1$). The flow rate ratio $q_R = q_2/q_1 = 1$, gap-to-thickness ratio $H_0/t = 3.33$ and dimensionless vacuum pressure $Vac = P_{vac}H_0/\sigma = 5$ are constant.

A close-up of the flow field in the coating bead region at three different values of the viscosity ratio $\mu_R = \mu_2/\mu_1$ is shown in Fig. 5. In this case, the flow rate ratio is $q_R = 1$, gap-to-thickness ratio $H_0/t = 3.33$, and vacuum pressure is $Vac = 5$. The blue color correspond to the liquid 1 or lower-layer liquid, $\phi = -1$. The red color represents the liquid 2 or upper-layer liquid, where $\phi = +1$. Upon exiting from the upstream feed slot, the bottom fluid layer would flow under the upstream die block, turn then to form the curved upstream meniscus and eventually come into contact with the web at the dynamic contact line, from there the liquid is accelerated in the web direction, rapidly approaching the web velocity. At viscosity ratio higher than unity, *i.e.* lower-layer liquid less viscous than upper layer liquid, the dynamic contact line is located far from the lower-layer feed slot. As the viscosity ratio falls, *i.e.* lower-layer liquid more viscous, the viscous stress becomes stronger dragging more liquid into the coating bead, and the dynamic contact line moves towards the lower layer feed slot. This changes has a weak influence in the downstream static contact angle. The recirculation present under the middle die lip gradually disappear and a large recirculation under the downstream die lip begins to appear. The two liquid layers contact at the separation line located at the upstream corner of the center die block.

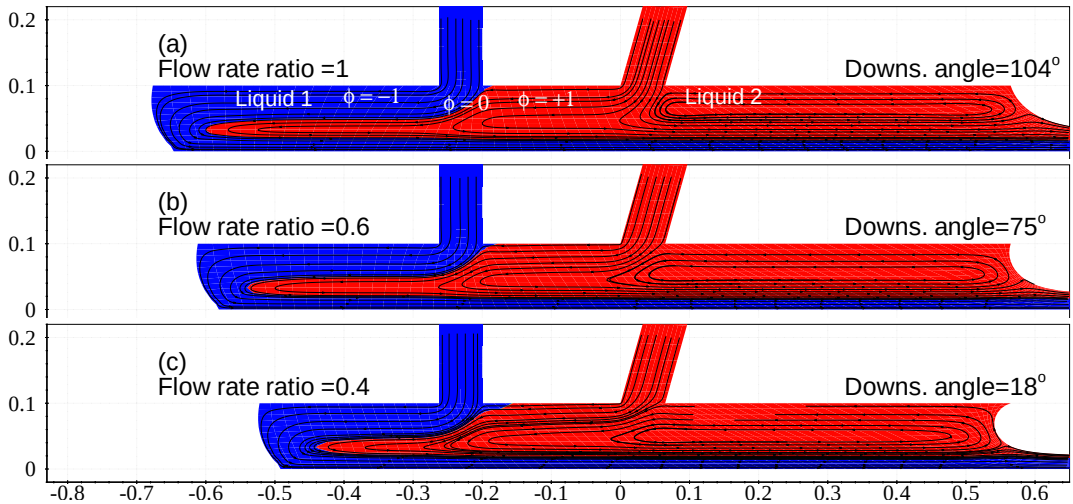

Figure 6. Flow field for different flow rate ratios, the gap-to-thickness ratios H_0/t are (a) 3.33, (b) 4.1 and (c) 4.8 respectively. Viscosity ratio $\mu_R = 0.25$ and $Vac = -14.2$ are constant.

Figure 6 shows the evolution of the flow field by lowering the flow rate ratio $q_R = q_2/q_1$ and rising the gap-to-thickness

ratio H_0/t at viscosity ratio $\mu_R = 0.25$ and vacuum pressure $Vac = -14.2$. The reduction of the upper layer flow rate q_2 changes the force balance in the downstream meniscus, it becomes more curved (smaller radius of curvature) in order to increase the adverse pressure gradient under the free surface. Because of the high gap-to-thickness ratio ($H_0/t > 3$) a large recirculation is present under the downstream die lip extending along the middle and upstream die lip. Changes in the upper layer flow rate has a weak influence in the dynamic contact line position and size of the recirculation.

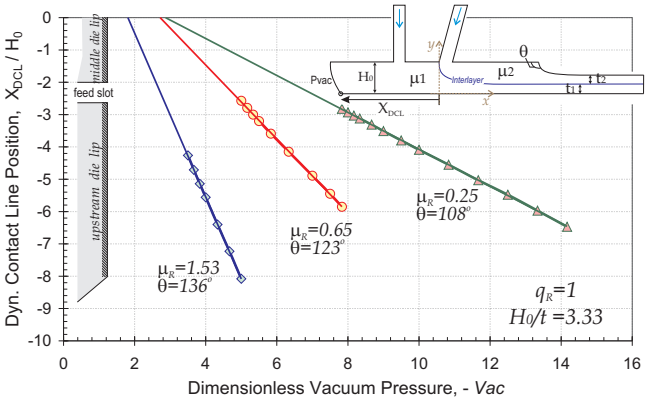

Figure 7. Dynamic contact line position as a function of vacuum pressure $Vac = P_{vac}H_0/\sigma$.

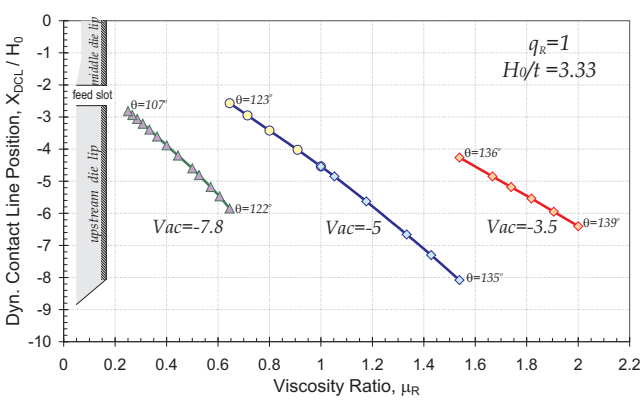

Figure 8. Dynamic contact line position as a function of the viscosity ratio $\mu_R = \mu_2/\mu_1$.

The position of the dynamic contact line as a function of the vacuum pressure Vac and viscosity ratio μ_R is illustrated in Figs. 7 and 8 at constant flow rate ratio $q_R = 1$ and gap-to-thickness ratio $H_0/t = 3.33$. As expected, too great the vacuum (applied at the upstream meniscus) causes liquid to be draw along the upstream die surface into the vacuum chamber, located in $X_{DCL}/H_0 = -8$ as indicated in the figure. Higher vacuum is required in order to keep the dynamic contact line close to the upstream edge of the upstream die lip, as the viscous of the bottom layer liquid rises. As shown in Fig. 9, the downstream static contact angle between the free surface and the downstream die land is almost insensitive to accentuated changes in the bottom layer and upstream meniscus conditions.

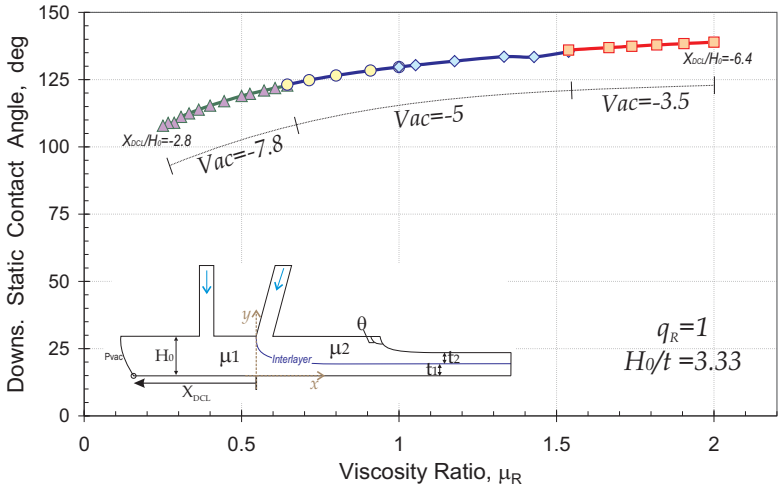

Figure 9. Downstream static contact angle as a function of the viscosity ratio $\mu_R = \mu_2/\mu_1$.

Figures 10 and 11 shows the position of the dynamic contact line X_{DCL}/H_0 as a function of the gap-to-thickness ratio $H_0/(t_1 + t_2)$ at low ($\mu_R = 0.25$) and high ($\mu_R = 2$) viscosity ratio. As the gap-to-thickness ratio increases, *i.e.* total film thickness diminishes, the dynamic contact line moves toward the upstream feed slot located between $-2.6 \leq X_{DCL}/H_0 \leq 2$ decreasing the coating bead length. The sensitivity of the dynamic contact line to changes in the film thickness is more intense when the flow rate ratio $q_R = q_2/q_1$ increases, *i.e.* upper layer flow rate q_2 is kept constant and the lower layer flow rate q_1 lowered, as is shown in Fig. 10 at $\mu_R = 2$ (lower layer liquid less viscous). In the same figure, opposite behavior is observed when the lower layer liquid is more viscous $\mu_R = 0.25$, the dynamic contact line moves toward the vacuum box when the total film thickness falls (gap-to-thickness ratio increases). This behavior is recorded at low ($Vac = -8.2$) and high ($Vac = -14.2$) vacuum level.

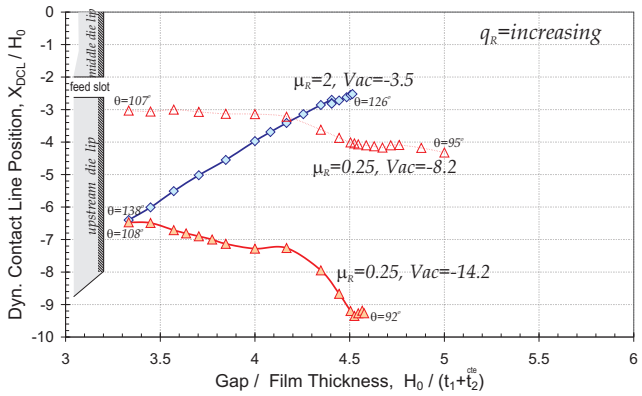

Figure 10. Dynamic contact line position as a function of the gap-to-thickness ratio $H_0/(t_1 + t_2)$, $t_2 = constant$.

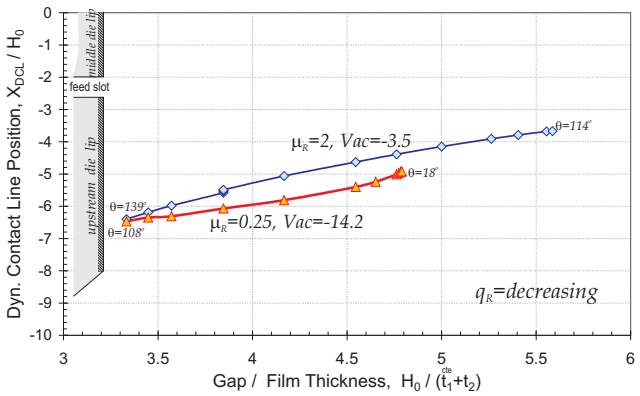

Figure 11. Dynamic contact line position as a function of the gap-to-thickness ratio $H_0/(t_1 + t_2)$, $t_1 = constant$.

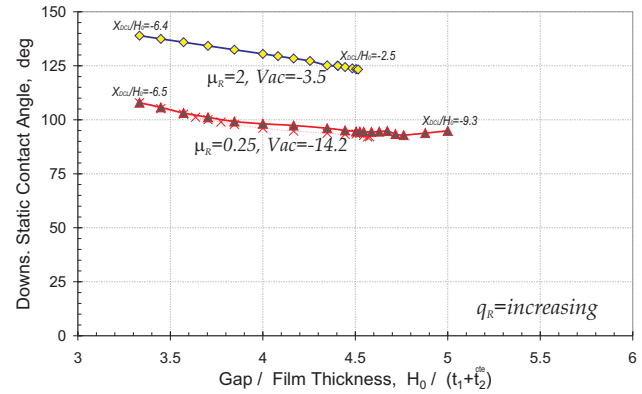

Figure 12. Influence of the lower layer flow rate q_1 in the downstream static contact angle.

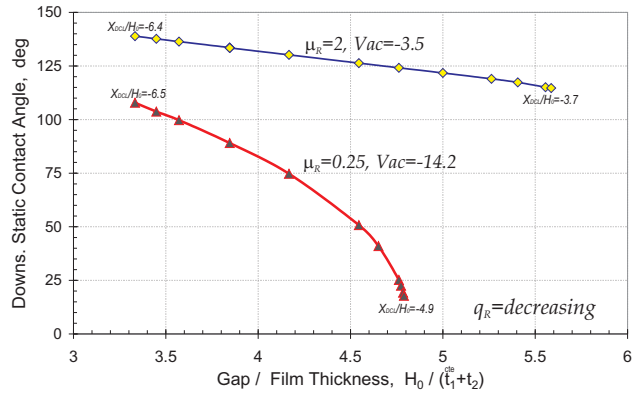

Figure 13. Influence of the upper layer flow rate q_2 in the downstream static contact angle.

The response of the downstream static contact angle is illustrated in Figs. 12 and 13 at equal conditions previously presented. When the flow rate ratio q_R is increased, keeping constant the upper layer flow rate q_2, the contact angle decreases slightly. At viscosity ratio $\mu_R = 0.25$ (lower layer liquid more viscous) and lowering the upper layer flow rate q_2 the contact angle diminishes markedly and the meniscus recedes toward the slot gap until the low-flow limit (Romero *et al.*, 2004) be identified at $H_0/t = 4.8$, *i.e* the meniscus curve so much that cannot bridge the gap clearance.

5. References

Osher, S.J. and Sethian, J.A., 1988, “Fronts propagating with curvature dependent speed: algorithms based on Hamilton-Jacobi formulations”, *J. Comput. Phys.*, 79, pp. 12-49.

de Santos, J.M., 1991, “Two-phase cocurrent downflow throught constricted passages”, PhD Thesis, University of Minnesota, MN, USA.

Musson, L.C., 2001, “Two-layer slot coating”, PhD Thesis, University of Minnesota, MN, USA.

Bolstad, J. H. and Keller, H. B., 1986, "A multigrid continuation method for elliptic problems whit folds”, *SIAM Journal of Scientific and Statistical Computing*, Vol **7**, issue 4, pp. 1081-1104.

Romero, O.J., Suszynski, W.J., Scriven, L.E and Carvalho, M.S., “Low-flow limit in solt coating of dilute solutions of high molecular weight polymer”, *J. of Non-Newtonian Fluid Mech.*, **118**, pp. 137-156, 2004.

6. Responsibility notice

The author(s) is (are) the only responsible for the printed material included in this paper